Journal of Visualized Experiments

Advanced self-healing asphalt reinforced by graphene structures: An atomistic insight

--Manuscript Draft--

Article Type:	Invited Methods Collection - JoVE Produced Video
Manuscript Number:	JoVE63303R2
Full Title:	Advanced self-healing asphalt reinforced by graphene structures: An atomistic insight
Corresponding Author:	Denvid Lau, Ph.D. City University of Hong Kong Hong Kong, Hong Kong CHINA
Corresponding Author's Institution:	City University of Hong Kong
Corresponding Author E-Mail:	denvid@mit.edu;denvid.lau@cityu.edu.hk
Order of Authors:	Fenghua Nie
	Wei Jian
	Denvid Lau, Ph.D.
Additional Information:	
Question	**Response**
Please specify the section of the submitted manuscript.	Engineering
Please indicate whether this article will be Standard Access or Open Access.	Standard Access ($1400)
Please indicate the **city, state/province, and country** where this article will be **filmed**. Please do not use abbreviations.	Hong Kong, China
Please confirm that you have read and agree to the terms and conditions of the author license agreement that applies below:	I agree to the Author License Agreement
Please confirm that you have read and agree to the terms and conditions of the video release that applies below:	I agree to the Video Release
Please provide any comments to the journal here.	

TITLE:

Advanced Self-Healing Asphalt Reinforced by Graphene Structures: An Atomistic Insight

AUTHORS AND AFFILIATIONS:

Fenghua Nie*, Wei Jian*, Denvid Lau

Department of Architecture and Civil Engineering, City University of Hong Kong, Hong Kong, China.

*These authors contributed equally to this work.

Email addresses of co-authors:

Fenghua Nie (fenghunie2-c@my.cityu.edu.hk)

Wei Jian (wjian6@cityu.edu.hk)

Denvid Lau (denvid.lau@cityu.edu.hk)

Corresponding author:

Denvid Lau (denvid.lau@cityu.edu.hk)

KEYWORDS:

asphalt, graphene, molecular dynamics simulations, self-healing

SUMMARY:

Graphene-modified asphalt nanocomposite has shown an advanced self-healing ability compared to pure asphalt. In this protocol, molecular dynamics simulations have been applied in order to understand the role of graphene in the self-healing process and to explore the self-healing mechanism of asphalt components from the atomistic level.

ABSTRACT:

Graphene can improve the self-healing properties of asphalt with high durability. However, the self-healing behaviors of graphene-modified asphalt nanocomposite and the role of incorporated graphene are still unclear at this stage. In this study, the self-healing properties of pure asphalt and graphene-modified asphalt are investigated through molecular dynamics simulations. Asphalt bulk with two crack widths and locations for graphene is introduced, and the molecular interactions among asphalt components and the graphene sheet are analyzed. The results show that the location of graphene significantly affects the self-healing behaviors of asphalt. Graphene near the crack surface can greatly accelerate the self-healing process by interacting with the aromatic molecules through π-π stacking, while graphene at the top area of the crack tip has a minor impact on the process. The self-healing process of asphalt goes through the reorientation of asphaltene, polar aromatic, and naphthene aromatic molecules, and the bridging effect of saturate molecules between the crack surface. This in-depth understanding of the self-healing mechanism contributes to the knowledge of the

enhancement for self-healing properties, which will help to develop durable asphalt pavements.

INTRODUCTION:

Deterioration under daily vehicle loadings and variant environmental conditions and the aging of asphalt during service results in degradation or even structural failures, i.e., cracking and raveling, which can further weaken the durability of asphalt pavements. The inherent response of asphalt to repair micro-cracks and voids automatically helps it recover from damages and restore strength[1]. This self-healing capability can considerably extend the service life of asphalt, save costs on maintenance, and reduce the emission of greenhouse gases[2,3]. The self-healing behavior of asphalt generally depends on several influencing factors, including its chemical composition, the degree of damage, and environmental conditions[4]. The improved self-healing capability of asphalt that can fully heal damage within a short period is desired; this has attracted extensive research interest in better mechanical performance and durability for asphalt pavements within civil engineering.

Novel methods to improve the self-healing capability of asphalt mainly include three approaches – inducing heating, encapsulation healing, and incorporating nanomaterials – which can be applied individually or simultaneously[5,6]. Inducing heating can significantly improve the mobility of asphalt and activate its self-healing for recovery[7]. The self-healing technology of asphalt by inducing heating can be ascribed to the assisted self-healing technique, which indicates that the self-healing properties of asphalt are improved by external stimuli. The objective of adding the steel wool fibers is to enhance the electrical conductivity and increase the healing capacity of the asphalt binder[8]. The approach to induce heat is to expose these electrically conductive fibers to the high-frequency alternating electromagnetic field, which can induce eddy currents, and the heat energy can diffuse into the asphalt binder by the conductive fibers[9]. The steel wool fibers are not just enhancing the electrical conductivity but also the thermal conductivity, which can both positively affect the self-healing properties of asphalt. However, it is challenging to select the proper mixing time for fibers[10]. The length of fibers decreases with increased mixing time and influences thermal conductivity, while the decreased mixing time leads to clusters of fibers and impedes the mechanical properties of asphalt[9]. The encapsulation method can supply light components of aged asphalt such as aromatics and saturates and refresh the self-healing capability of asphalt[11,12]. However, this is a once-only treatment, and the healing materials cannot be replenished after the release. With the development of nanotechnology, nanomaterials have become promising modifiers for enhancing asphalt-based materials. Asphalt binders incorporated with nanomaterials present better thermal conductivity and mechanical properties[13]. Graphene with excellent mechanical performance and high thermal performance is regarded as an excellent candidate to improve the self-healing ability of asphalt[14–17]. The increased healing properties of graphene-modified asphalt can be attributed to the fact that graphene increases the capacity of the asphalt binder to be heated and produce heat transfer inside the asphalt binder, which means that graphene-modified asphalt

can be heated more rapidly and reach up to higher temperature than pure asphalt[18]. The generated heat can be transferred throughout the graphene-modified asphalt at a faster speed than that through pure asphalt. The crack region of the asphalt binder can be influenced easily and healed faster by the heat flow with higher temperature and higher heating capacity. The self-healing reaction will begin if the energy that is equal to or larger than the healing activation energy exists at the crack surface of the asphalt[19]. Graphene can improve the thermal activation healing performance and accelerate the healing rate of asphalt[19,20]. Besides, graphene can save heating energy by up to 50% during the healing process, which can benefit energy efficiency and reduce maintenance costs[21]. As a microwave-absorbent material, graphene is reported to improve the healing ability of asphalt during the rest period of microwave heating[22]. It is expected that the addition of graphene into asphalt will improve not only the mechanical performance but also the self-healing and energy-saving capacity, which requires in-depth knowledge of the self-healing mechanism.

Self-healing at the nanoscale is mainly due to the wetting and diffusion of asphalt molecules at the fractured faces[23]. As asphalt consists of various polar and non-polar molecules, its self-healing capability is strongly related to molecular interactions and movements of the asphalt molecules of different components[1]. However, current research mainly relies on experimental techniques to quantify macroscopic mechanical properties, which causes missing information in the change of microstructures and the interactions between molecules in asphalt when trying to understand the healing mechanism. The reinforcing mechanism of graphene in the self-healing capability of asphalt is also unclear at this stage. Molecular dynamics (MD) simulations play an influential role in investigating molecular interactions and motions of nanocomposite systems, and link microstructural deformation with molecular interactions and movements[24–31]. MD simulations have become more and more popular for analyzing material behaviors that cannot be accessed easily by experiments[32,33]. Existing studies have shown the feasibility and availability of MD simulations in asphalt systems; the cohesion, adhesion, aging, and thermomechanical properties of asphalt and asphalt composites can be explored by MD simulations[34–37]. The self-healing behaviors of asphalt can also be predicted by MD simulations[38–40]. Therefore, it is believed that the investigation using MD simulations is an effective way to understand both the self-healing and reinforcing mechanisms.

The objectives of this study are to investigate the self-healing behaviors of pure asphalt and graphene-modified asphalt nanocomposites and to understand the role of graphene in improving the healing capacity of asphalt through MD simulations. The self-healing simulations of pure asphalt and graphene-modified asphalt composites are carried out by introducing cracks into the initial structures. The self-healing capabilities are characterized by the contour of atom numbers, the reorientation and entanglements of molecules at the fractured face, and the mobility of asphalt components during the self-healing processes. By investigating the healing efficiency of graphene at different sites, the reinforcing mechanism of graphene contributing to the self-healing abilities of asphalt is unveiled, which can help with the monitoring of nanofillers in an optimal way and thus enable the life extension of

asphalt pavements. An investigation of the self-healing capacity at the atomistic scale can provide an efficient way to develop advanced asphalt-based materials for future research.

According to asphalt chemistry, asphalt consists of various types of hydrocarbons and non-hydrocarbons with different polarity and shapes, which can mainly be divided into the four components of asphaltene, polar aromatics, naphthene aromatics, and saturates[41,42]. Asphaltene molecules are relatively larger and heavier than other molecules in asphalt, with a mean atomic mass of roughly 750 g/mol and a molecular diameter in the range of 10–20 Å. It has been widely accepted that asphaltene is composed of large aromatic cores that contain heteroatoms and are surrounded by different lengths of alkyl groups[43]. A modified asphaltene molecule is constructed, as shown in **Figure 1a**. The molecules of polar aromatics and naphthene aromatics are constructed based on the polarity and the element ratio of asphalt molecules, with benzobisbenzothiophene ($C_{18}H_{10}S_2$) representing the polar aromatic molecule and 1,7-dimethylnaphthalene ($C_{12}H_{12}$) chosen as the representative naphthene aromatic molecule, as shown in **Figure 1b–c**. *N*-docosane (*n*-$C_{22}H_{46}$) is constructed as shown in **Figure 1d**. The parameters listed in **Table 1** for asphalt molecules are selected and used to meet the desired criteria, including the elemental mass fraction, the atom ratio, and the aromatic/aliphatic ratio, of real asphalt from experiments[41]. The same mass ratio has been defined in our previous studies, and the other thermomechanical properties like density, glass transition temperature, and viscosity are in good agreement with experimental data of real asphalt[36]. The molecular structure of graphene applied in this study is shown in **Figure 1e**. The adopted graphene sheet in this study has no defect and no fold compared to that of the real case, while the real graphene sheet usually has several defects such as the atomic vacancies and Stone-Wales defects[44], and some of the graphene sheets can be folded during the mixing process with the asphalt matrix[45]. These imperfect situations are not considered in this study, since we focus on the effect of the site of the graphene sheet on the self-healing properties and choose it as the only variable in this study. The variables of graphene sheets in terms of the defects and folded cases will be the focus of our future studies. The mass ratio of graphene to asphalt in this study is 4.75%, which is the normal situation (<5%) for graphene modified asphalt in the experiment[46,47].

[Place **Figure 1** here]

[Place **Table 1** here]

With respect to the protocol described below, two types of wedge-like cracks with different sizes are inserted into the middle of the asphalt model with a blunt crack tip and two parallel crack surfaces, while the middle-top area of the asphalt bulk remains intact. Two crack widths are chosen as 15 Å and 35 Å, as shown in **Figure 2a–b**. The reason for selecting 15 Å is that the crack width should be wider than the cutoff of 12 Å to avoid the early self-healing of asphalt molecules during the equilibrium process while investigating an extreme case for a small crack. The reason for selecting 35 Å is that the crack width should be wider than the

length of the saturate molecules of 34 Å in order to prevent the bridging effect. The height of the crack is 35 Å, the same as the box width, and the depth of the crack is 70 Å, the same as the box length. In the real situation, the observed micro-crack sizes can be varied in the range from several micrometers to several millimeters, which is far larger than the length scale we are modeling here. Normally, the length scale in MD simulation is limited to the scale of 100 nm, which is still several orders of magnitude smaller than the real crack size. However, the cracks initiate at the nanoscale and grow into macroscale cracks with continuous deformation[48]. The understanding of the self-healing mechanism at the nanoscale can help to prevent the growth and further propagation of the crack at the macroscale. Even though the selected crack sizes are in the range of nanometer, the results can still be influential and applicable to explore the self-healing behaviors of asphalt molecules. There are two locations for the graphene sheets in the crack areas: one is on top of the crack tip and the other is perpendicular to the left crack surface. It has been found that these are the most common positions for graphene in graphene-modified nanocomposites with cracks[49].

[Place **Figure 2** here]

In MD simulations, the intramolecular and intermolecular interactions in the asphalt nanocomposites are described by the Consistent Valence Forcefield (CVFF)[50], which works well with asphalt and graphene-based materials. The functional form of CVFF has the following expression:

$$E_{total} = \sum_b K_b (b - b_0)^2 + \sum_\theta K_\theta (\theta - \theta_0)^2 + \sum_\phi K_\phi [1 + s\cos(n\varphi)] + \sum_\chi K_\chi [1 - \cos(2\chi)] + \sum_{nonbond} \left\{ \varepsilon_{ij} \left[\left(\frac{r_{ij}^o}{r_{ij}} \right)^{12} - \left(\frac{r_{ij}^o}{r_{ij}} \right)^{6} \right] + \frac{q_i q_j}{\varepsilon_0 r_{ij}} \right\} \quad (1)$$

Here, the total energy E_{total} is composed of the bonded energy terms and the non-bonded energy terms. The bonded interactions consist of the covalent bond stretching, the bond angle bending energy, the torsion angle rotation, and the improper energies as expressed in the first four terms. The non-bonded energy includes an LJ-12-6 function for the van der Waals (vdW) term and a Coulombic function for the electrostatic interactions. CVFF has been widely employed in simulating asphalt materials[51,52]. The simulated physical and mechanical properties such as density, viscosity, and bulk modulus are in good agreement with the experimental data, which demonstrates the reliability of CVFF[51]. CVFF is not only suitable for inorganic materials, but it has also been successfully employed in structures consisting of organic and inorganic phases such as asphalt-silica[52] and the system of epoxy-graphene[53]. In addition, the interfacial interactions between graphene and asphalt can be characterized with CVFF[36,54]. Since the major part in selecting forcefield is to determine the asphalt-graphene interface, the non-bonded interactions described by CVFF are more reliable, which is also considered in our previous study[36]. Overall, the forcefield CVFF is adopted in this study. The partial charges for different kinds of atoms are calculated by the forcefield-assigned method.

PROTOCOL:

1. **Build the atomistic models**

1.1 Open the Materials Studio software to create five 3D atomistic documents and rename these documents as graphene, asphaltene, polar aromatics, naphthene aromatics, and saturates, respectively.

1.2 Build the graphene model by creating the unit cell of graphene sheet in the 3D atomistic document using the **Sketch Atom** option.

1.3 Construct the final structure using the Supercell option in the **Build > Symmetry** menu. Define the size of the graphene sheet as 40 Å x 40 Å, which is larger than the asphalt chains and the crack width.

1.4 Build and pack the four types of asphalt molecules.

1.4.1 Use the **Sketch Atom** option to draw the molecular structures of asphaltene, polar aromatics, naphthene aromatics, and saturates separately.

1.4.2 Pack the four kinds of asphalt molecules into the simulation box using the **Calculation** option in the **Modules** > **Amorphous Cell** menu.

1.5 Build the asphalt structure with the crack.

1.5.1 Set the height of the crack zone in the x dimension the same as the height of the box of 70 Å and the depth of the crack zone in the y dimension is half of the height of the box as 35 Å.

1.5.2 Set two cases of the crack widths in the z dimension of 15 Å and 35 Å. Delete the redundant molecules in the crack zones of the middle-down area of asphalt bulk using the **Delete** option and keep the asphalt matrix in the middle-up area unchanged.

1.6 Build the graphene-modified asphalt structure with the crack. Incorporate the graphene sheet into the top area of the crack tip and the left crack surface separately before the packing step using the **Copy** + **Paste** command.

1.7 Pack the asphalt molecules into the simulation box based on the final compositions listed in **Table 1** to construct the graphene-modified asphalt structure.

1.8 Convert the structure file to a data file. Save the structure files as the molecule files with structure information (*.car and *.mdf) from Materials Studio. Convert the molecule files (*.car and *.mdf) to data files using the msi2lmp tool in large-scale atomic/molecular

massively parallel simulator (LAMMPS)[55] package. Read the data file by the **read_data** command in LAMMPS.

2. **Perform the simulations**

2.1 Define the parameters of the simulations.

2.1.1 Set the timestep as 1 fs in the input file considering the balance of accuracy and efficiency of the carried simulations.

2.1.2 Set the cutoff distance of non-bonded interactions as 12 Å, which is less than half the length of the simulation box in consideration of the periodic boundary condition and the calculational efficiency.

2.1.3 Employ the particle-particle particle-mesh (PPPM) algorithm to describe the long-range Coulombic interactions and set the relative error in per-atom forces calculated by the long-range solver as 10^{-5} for high accuracy.

2.2 Fix the profile of crack. Select the asphalt molecules on the profile by the **Group Molecules** command in LAMMPS. Apply the constraints on the asphalt molecules using the **Fix Spring/Self** command in LAMMPS to avoid the movements of asphalt molecules.

2.3 Achieve the equilibrium

2.3.1 Keep the whole simulation box fully relaxed after 500 ps under the isothermal-isobaric (NPT) ensemble with a temperature of 300 K and pressure of 1 atm.

2.3.2 Make the asphalt bulk equilibrated to the desired density value of the experimental measurements of 0.95–1.05 g/cm^3[3,41] by continuously examining the temperature, pressure, density, and energy values using the **Thermal** command.

2.3.3 Check the convergence of potential energy and the mean-squared displacement (MSD) in the whole system for achieving the fully relaxed state.

2.4 Perform the self-healing process.

2.4.1 Set the whole simulation box under the NPT ensemble with a temperature of 300 K and pressure of 1 atm.

2.4.2 Remove the constraint of the asphalt molecules on the contour of the crack zone.

2.4.3 Track and record the size of the simulation box and the coordinates of atoms and use

the **Dump** command for postprocessing.

2.4.4 Average the simulation results during the self-healing process over three independent configurations with three different initial velocity seeds in order to decrease the random errors.

3. Postprocessing

3.1 Visualize the self-healing behaviors. Open the Open Visualization Tool OVITO[56] to visualize the simulation progress, and then open the trajectory files in the lammpstrj format generated by LAMMPS[55]. Record the snapshots of the self-healing process and track the paths of asphalt molecules using the **Render** command.

3.2 Analyze the contour of the atom number. Export the coordinates of the atoms to data analysis and graphing software from the trajectory files outputted from LAMMPS. Project the coordinates of atoms in the whole system onto the yz plane. Record atom numbers at different areas of the yz plane and plot the contour with different colors.

3.3 Analyze the atom mobility and relative position.

3.3.1 Analyze the atom mobility of different asphalt components by the mean-squared displacement (MSD) using the **Compute msd** command.

3.3.2 Calculate the relative positions between graphene and asphalt molecules by the radial distribution functions (RDF) curves for the system of graphene-modified asphalt systems with the 15 Å and 35 Å crack widths using the **Compute rdf** command in LAMMPS.

3.3.3 Draw the RDF curves to check how the density of asphalt varies as a function of distance from the graphene sheet.

REPRESENTATIVE RESULTS:

The contour of atom number

The contours of the atom number of pure asphalt and graphene-modified asphalt models in the yz plane are shown in **Figure 3**, where the color bar from blue to red exhibits atom numbers varying from 0 to 28. **Figure 3a–c** illustrates the contour of the atom number of the structures with 15 Å crack width in pure asphalt, graphene-modified asphalt at the crack tip, and graphene-modified asphalt at the crack surface. For pure asphalt, complete healing occurs after about 300 ps. The self-healing behavior starts from the area of the crack tip, as the area around the crack tip becomes a melted blunt shape with a blue color after 50 ps, and several asphalt molecules bridge the two crack surfaces at the middle of the crack tip. The green color in the contour presents the bulk asphalt, which is the stage of the crack zone following self-healing. At around 100 ps, the crack zone is almost closed with a small void left, and the colors

of the initial crack surfaces change to green, which indicates that the self-healing process is finished in these areas; however, there are still some blue and white areas remaining to be self-healed. After about 300 ps, most of the color of the crack zone has changed to green, which is the same as that of the asphalt bulk, indicating that the self-healing process is complete. As shown in **Figure 3b**, the self-healing process is not significantly changed after adding the graphene sheet on the top of the crack. The self-healing process takes about 500 ps to complete, and the crack zone is sharply decreased at 50 ps and almost disappears at 200 ps. The graphene sheet on the top of the crack tip seems to have little influence on the self-healing process of the crack surface. However, inserting the graphene in the left of the crack surface can significantly accelerate the self-healing process, as shown in **Figure 3c**, where the red line in the contour is the graphene sheet. The self-healing period is shortened to around 200 ps, which is half as much as that of pure asphalt. The crack width is significantly decreased at 20 ps, and the asphalt molecules from the bulk tend to move to the graphene area and fill up the crack area. The crack zone almost disappears at around 150 ps, although some of the areas at the bottom remain blue. After another 50 ps of the self-healing process, the crack area is full of blue color, which indicates the end of the process.

The self-healing process of the models with 35 Å crack width takes almost twice as long as that of the models with 15 Å crack width, while the self-healing process of pure asphalt lasts around 1,000 ps. The self-healing behavior starts in the crack tip area, and the crack shape becomes shrunken and irregular at 100 ps. Most of the crack zone is healed by 500 ps, with a small void left in the middle of the crack zone. After performing the self-healing process for another 500 ps, the crack zone is filled with asphalt molecules until the self-healing process is completed. The graphene sheet is located on the top of the crack tip, as shown by the red line of **Figure 3e**. The self-healing period is about 1,100 ps, which is close to that of pure asphalt. However, the crack shape changes differently. There are some asphalt molecules that bridge the crack area at around 400 ps, which can advance the self-healing process. As shown in **Figure 3f**, the self-healing behaviors can be significantly improved when the graphene sheet is located at the left crack surface. A phenomenon can be observed similar to the model with 15 Å crack width: some of the asphalt molecules in the asphalt bulk tend to move to the graphene area and wrap around the graphene sheet, which can decrease the crack area significantly and help the self-healing process. The width of the crack is decreased to around half of the initial crack width by only 50 ps, and most of the crack area is healed at around 300 ps. The whole self-healing process lasts about 600 ps and most of the crack zone disappears; this takes only half the length of time taken by pure asphalt.

[Place **Figure 3** here]

Molecular interactions

To explore the difference in self-healing behaviors between pure asphalt and graphene-modified asphalt composites, the molecular interactions and movement during the self-healing process are captured and analyzed, as shown in **Figure 4**. From **Figure 4a**, it can be

observed that aromatic molecules like asphaltene, polar aromatics and naphthene aromatics are attracted by the graphene sheet through π-π stacking when graphene is placed on the top area of the crack tip. These asphalt molecules are captured tightly by the graphene sheet and cannot readily diffuse into the neighborhood of the crack zone or fill up the crack, which hinders the self-healing process to a certain extent. However, the self-healing behaviors mainly arise from the asphalt molecules near the crack surface, and the influence of these molecules in the top area needs further exploration. From **Figure 4b**, it is observed that the polar aromatic molecule at the crack surface is attracted by the graphene sheet at the other crack surface, which can further increase the nearby naphthene aromatic molecule's likelihood of moving onto the crack area. The gathered asphalt molecules attracted by the graphene sheet can pack the crack zone with a higher speed than that of pure asphalt and the self-healing ability of the graphene-modified asphalt nanocomposite can be improved. The self-healing process of the model with 35 Å crack width modified by graphene at the left crack surface is shown in **Figure 4c**. The polar aromatic molecules are attracted by the graphene sheet through π-π stacking when the self-healing begins, and these asphalt molecules can rapidly wrap around the graphene sheet and reduce the space of the crack zone, as shown in **Figure 3f**. This indicates that graphene plays an important role in the initial stage of self-healing when it is located around the crack surface. A self-healing snapshot of pure asphalt with 15 Å crack width is shown in **Figure 4d**. It can be clearly observed that the chain structure of saturate is important for the self-healing process since the molecules can become entangled with each other and bridge the crack surface. This bridging effect between saturate molecules and the side chains of asphaltene molecules can significantly increase the packing efficiency and decrease the self-healing period. It is also observed that asphalt molecules with polyaromatic rings, such as asphaltene, polar aromatics, and naphthene aromatics, reorientate themselves at the crack surface by π-π stacking. This reorientation allows the asphalt molecules to move in a parallel direction and contributes to crack wetting, which further closes the crack surfaces.

[Place **Figure 4** here]

The reorientation of aromatic molecules including asphaltene, polar aromatics, and naphthene aromatics around the crack surface during the self-healing process, is shown in **Figure 5**. **Figure 5a** shows that the tracked molecules before self-healing are almost perpendicular between naphthene aromatics and polar aromatics and between asphaltene and polar aromatics. The distance between asphaltene and the other two aromatic molecules is 13.3 Å, which is larger than the distance between the aromatic molecules. After self-healing for 40 ps, the naphthene aromatic molecule diffuses to the space between asphaltene and polar aromatics and plays an important role in interacting with the other two molecules. In **Figure 5b**, it can be observed that the distance and angle between the polar aromatic molecule and naphthene aromatic molecule are 4.6 Å and 89°, which indicates a T-shaped π–π stacking interaction between the two aromatic molecules. The angle and distance between the naphthene aromatic and asphaltene decrease to 32° and 4.6 Å, respectively. This indicates

that the non-bond interactions between naphthene aromatics and asphaltene cause them to rotate and adjust the orientation gradually, contributing to the wetting of the crack surface. The orientations of the three molecules are almost parallel after 50 ps, as the angles between them are 26° and 35°, as shown in **Figure 5c**. The distance between them declines below 4.0 Å, which indicates that the π–π stacking facilitates the parallel structure and brings the aromatic molecules closer together. Overall, the reorientation at the crack surface promotes the interaction of asphalt molecules, which shortens the intermolecular distance and increases the attraction among them. The reorientation and diffusion of asphalt molecules further aid the filling up of the crack zone and speed up the self-healing process.

[Place **Figure 5** here]

Mobility of asphalt components

To understand the roles of different components quantitatively in the self-healing behaviors of asphalt, the MSD of the center mass for asphalt composite is calculated to represent the transitional mobility during the self-healing process, which is expressed by:

$$\mathrm{MSD}(t) = \left\langle \Delta r_i(t)^2 \right\rangle = \left\langle (r_i(t) - r_i(0))^2 \right\rangle \quad (4)$$

where $r_i(t)$ is the position vector of particle i at time t, and the angular bracket indicates the average value of the traveling distance. The MSD values of pure asphalt and graphene-modified asphalt are tracked and shown in **Figure 6**. **Figure 6a–c** shows the MSD of asphalt composite with a 15 Å width crack, while those with a 35 Å width crack are shown in **Figure 6d–f**. It can be observed that saturates are the most active component in the self-healing behaviors of asphalt, while asphaltene is the least active. There are two possible reasons: one relates to the molecular mass, as asphaltenes have the highest molecular mass in asphalt, and they are less able to move and fill the crack zone. The other is the chain-like structure of saturates, which have higher mobility than other components and are more likely to become entangled and stretch out at the crack surface. The mobility of polar aromatics is higher than that of naphthalene aromatics; this is because of the higher molecular mass and polarity of polar aromatics. The polar atoms on polar aromatics, such as sulfur atoms, can form an H-bond with asphaltenes, and the mobility can be impeded. The MSD figures for graphene-modified asphalt on the top area of the crack tip and the left crack surface are shown in **Figure 6b** and **Figure 6c**. It can be seen in **Figure 6b** that the MSD of graphene is lower than those of asphalt components since graphene occupies the largest volume and has the highest molecular mass in the asphalt nanocomposites. The MSD values of asphalt components are relatively lower than those of pure asphalt; this is because the interactions among these molecules and graphene hinder the mobility of the asphalt molecules and slow the self-healing process. However, when graphene is placed at the left crack surface, the mobilities of polar aromatics, naphthene aromatics, and graphene improve significantly compared to that of pure asphalt. This indicates that graphene plays an important role in the self-healing process and that its interactions with aromatic molecules in asphalt contribute to the self-healing process of asphalt. For the 35 Å width crack case in **Figure 6d**, the MSD of pure asphalt

follows a similar trend to that of the case with 15 Å crack width, as the MSD of asphaltene, polar aromatics, naphthene aromatics, and saturates vary in an increasing manner. When inserting graphene into the top area of the crack tip, the MSD of saturates decreases by about 15 $Å^2$, which is more than that of pure asphalt. The existence of graphene sheets in asphalt bulk vertically influences the mobile space of the saturate molecules and prevents the routes of self-healing. From **Figure 6f**, it can be observed that the MSD values of asphaltene, polar aromatics and naphthene aromatics are all improved compared to pure asphalt, while the MSD of saturates decreases slightly. Graphene is highly responsible for the improvement of the self-healing process, especially with molecules containing aromatics. The π-π stacking interactions among graphene and asphaltene, polar aromatics, and naphthene aromatics improve the mobility of these asphalt molecules and help to form a stable packing structure in the crack zone, which accelerates the self-healing process of asphalt.

[Place **Figure 6** here]

Molecular locations after self-healing

To explore the relative locations between graphene and asphalt molecules during the self-healing process, the radial distribution functions between graphene and aromatic molecules in asphalt are calculated and shown in **Figure 7**. **Figure 7a–c** shows the RDF of the model with 15 Å crack width before and after the self-healing process. It can be seen that the aromatic molecules in asphalt move closer to the graphene sheet following the self-healing process, especially the polar aromatic molecules and naphthene aromatic molecules. As indicated in **Figure 4**, there are strong π-π stacking interactions between graphene and aromatic molecules such as asphaltene, polar aromatics, and naphthene aromatics, which cause the graphene sheet to attract these molecules toward the crack surface. However, the difference in the $g(r)$ values of asphaltene before and after self-healing is not as significant as those of polar aromatics and naphthene aromatics. This is because the asphaltene molecules obtain a higher molecular mass and volume than the polar aromatic and naphthene aromatic molecules, making it harder for them to rotate and diffuse to the graphene area and fill the crack zone. The increased $g(r)$ values between graphene and polar aromatic or naphthene aromatic molecules within 4.0 Å are within the typical interaction distance for π-π stacking, and the increased $g(r)$ values beyond 4.0 Å are due to the combination of molecular interactions and the elimination of the crack zone. An RDF of the model with 35 Å crack width before and after the self-healing process is shown in **Figure 6d–f**. The $g(r)$ values between graphene and asphaltene beyond 4.0 Å through the self-healing process are more obvious than those of the 15 Å crack width; this is because asphaltene has more space to diffuse and move toward the graphene in the larger crack zone. The $g(r)$ values within 4.0 Å are more significant for naphthene aromatics than those for polar aromatics; this is due to the smaller molecular mass and better diffusion ability of naphthene aromatic molecules.

[Place **Figure 7** here]

FIGURE AND TABLE LEGENDS:

Figure 1: **Chemical structure**. The atomistic models of (**a**) asphaltene molecule ($C_{53}H_{55}NOS$), (**b**) naphthene aromatic molecule ($C_{12}H_{12}$), (**c**) polar aromatic molecule ($C_{18}H_{10}S_2$), (**d**) saturate molecule ($C_{22}H_{46}$), (**e**) graphene, and (**f**) pure asphalt. For the atomistic asphalt model, the carbon, oxygen, nitrogen, sulfur, and hydrogen atoms are shown in gray, red, blue, yellow, and white, respectively.

Figure 2: **The self-healing schemes for pure asphalt and graphene-modified asphalt.** The self-healing model of pure asphalt with a crack width of (**a**) 15 Å and (**b**) 35 Å. The self-healing model of graphene-modified asphalt with the graphene sheet is located (**c**) at the top of the crack tip and (**d**) perpendicular to the crack surface.

Figure 3: The contour of the atom number during the self-healing process. The contour of the atom number during the self-healing process for the models with 15 Å crack width for (**a**) pure asphalt, (**b**) graphene on the crack tip, and (**c**) graphene at the left surface of the crack tip, and the models with 35 Å crack width for (**d**) pure asphalt, (**e**) graphene on the crack tip, and (**f**) graphene at the left surface of the crack tip. The dotted black boxes refer to the locations of graphene. The color bar from blue to red stands for the atom numbers varying from 0 to 28 in the contour.

Figure 4: Details of non-bond interaction of pure asphalt and graphene-modified asphalt nanocomposites during the self-healing process. For the model with (**a**) 15 Å crack width and graphene located on the top of the crack tip, aromatic molecules in asphalt are attracted by the graphene sheet through π-π stacking. For the model with (**b**) 15 Å crack width and graphene at the left side of the crack surface, the polar aromatic molecules at the other crack surface move onto the graphene surface due to strong aromatic interactions. For the model with (**c**) 35 Å crack width and graphene at the left side of the crack surface, the polar aromatic molecules are attracted by the graphene sheet and thus protrude from the crack surface. For the model with (**d**) 15 Å crack width and pure asphalt, there is a reorientation of aromatic molecules at the crack surface and a chain bridging and entanglement of saturate molecules during the self-healing process. The blue dotted boxes and purple dotted boxes in the figure indicate the π-π stacking and reorientation behaviors, respectively.

Figure 5: The reorientation of asphalt molecules during the self-healing process. Angles and distances among asphalt molecules (**a**) before self-healing, (**b**) after 40 ps, and (**c**) at 50 ps.

Figure 6: MSD of pure asphalt and graphene-modified asphalt molecules during the self-healing process. For the models with 15 Å crack width, MSD of (**a**) pure asphalt and graphene-modified asphalt on (**b**) the top of the crack tip and (**c**) the left surface is presented. For the models with 35 Å crack width, MSD of (**d**) pure asphalt and graphene-modified asphalt on (**e**) the top of the crack tip and (**f**) the left crack surface is presented. The X-axis represents the time of the simulation and the Y-axis represents the MSD values of asphalt components and

the graphene molecule during the self-healing process.

Figure 7: The RDF values between graphene at the left crack surface and the asphalt components. The RDF values between graphene at the left crack surface and the asphalt components of (**a**) asphaltene, (**b**) polar aromatics, (**c**) naphthene aromatics from the model with 15 Å crack width, (**d**) asphaltene, (**e**) polar aromatics, and (**f**) naphthene aromatics from the models with 35 Å crack width. The X-axis represents the distance of the two molecules and the Y-axis represents the RDF values.

Table 1: **Overall components of pure asphalt model and graphene-modified asphalt model.**

DISCUSSION:

The critical steps within the Protocol part are as follows: step 1.4 – Build and pack the four types of asphalt molecules; step 1.5 – Build the asphalt structure with the crack; step 2.3 – Achieve the equilibrium; step 2.4 – Perform the self-healing process. These steps indicate the most cohesive and important contents of the protocol. To create the desired shapes of the inserted crack, the packing process is modified compared to the normal packing in Materials Studio. The crack shape is created and filled inside the simulation box, and then the asphalt molecules are packed into the other part of the simulation box. After that, the redundant asphalt molecules are deleted around the created crack contour. The limitation of MD simulations is that the time scale and length scale are relatively small in the order of nanosecond and nanometer compared to traditional methods such as the finite element method, in which the simulations can be analyzed up to seconds and meters[57]. The significance of this method is that it can reveal the self-healing mechanism of asphalt and graphene-modified asphalt at the atomistic level by capturing nanostructure evolution, molecular interactions, and motions, which are hard to be accessed by traditional approaches[58]. The self-healing mechanism can help researchers and engineers to apply nanomaterials at the appropriate site and improve asphalt in an efficient way. The future application of this technique is that it can monitor the molecular structure in a decent manner and help to investigate the effect of other variables of nanomaterials such as defects, folded structures, and functional groups. This technique can also be combined with other approaches to observe the self-healing behaviors of asphalt nanocomposites from a multiscale aspect. The self-healing properties of asphalt can be understood thoroughly and get improved significantly in the future.

Graphene is critical in the changes and migration of the interface and components during the self-healing process. Without inserting the graphene sheet, saturate plays an important role in the self-healing process, since the chain structure of saturates can entangle with each other and bridge the crack surface. The bridging effect between saturate molecules and the side chains of asphaltene molecules can strongly increase the packing density and decrease the time of the self-healing process. Besides, asphalt molecules with polyaromatic rings, such as asphaltene, polar aromatics, and naphthene aromatics, reorientate themselves at the crack

surface by π-π stacking, which makes the asphalt molecules move in a parallel direction and contributes to crack wetting and closes the crack surfaces. With the insertion of graphene, the polar aromatic molecules at one side of the crack surface are attracted by the graphene sheet at the other side of the crack surface, which can further increase the possibility of nearby naphthene aromatic molecules moving into the crack area. The gathered asphalt molecules attracted by the graphene sheet can fill in the crack zone with a higher speed than that in pure asphalt, and the self-healing ability is significantly improved in the graphene-modified asphalt nanocomposite. Asphaltene molecules have higher molecular mass and volume in the asphalt matrix, which makes them hard to diffuse to the graphene part and fill in the crack zone. Naphthene aromatics have faster movement than polar aromatics, which is due to the smaller molecular mass and better diffusion ability of naphthene aromatic molecules[39].

In this study, the self-healing properties of pure asphalt and graphene-modified asphalt nanocomposites are investigated in consideration of different crack widths and graphene locations using MD simulations. It is observed that the self-healing behavior starts from the crack tip area, with the sharp tip becoming blunt and fuzzy. Asphalt molecules at the crack boundary can diffuse to decrease the width of the crack and continue filling the gap. The complete self-healing process is confirmed when the atom density of the crack area is the same as that of the asphalt bulk. MD simulations can help to reveal the molecular interactions and the chain movement in the asphalt matrix during the self-healing process. The entanglement and reorientation of asphalt molecules play an important role in self-healing behaviors. The self-healing rate with the incorporation of the graphene sheet is determined by its location. For the graphene sheet located at the crack tip area, the movement of the asphalt molecules is hindered and cannot easily diffuse into the crack zone. For the graphene sheet at the side of the crack zone, the asphalt molecules are attracted by the graphene sheet due to π-π stacking interaction and easily gather at the crack zone, indicating an increasing self-healing rate. The simulation results show that the modification of asphalt by nanomaterials can improve both thermomechanical and self-healing properties, which has great potential for the development of smart asphalt pavements. The fundamental understanding of the self-healing mechanism in asphalt nanocomposites based on MD simulations can facilitate efficient manipulation of nanomaterials at the optimal site, which is beneficial to the advanced design of asphalt nanocomposites with desired properties and functions.

ACKNOWLEDGMENTS:

The authors are grateful for the support from the Research Grants Council (RGC) of the Hong Kong Special Administrative Region, China, with Project No. R5007-18, and the support from Shenzhen Science and Technology Innovation Committee under the grant JCYJ20170818103206501.

DISCLOSURES:

The authors have no conflicts of interest to declare.

REFERENCES:

1. Sun, D. et al.A comprehensive review on self-healing of asphalt materials: Mechanism, model, characterization and enhancement. *Advances in Colloid and Interface Science*. **256**, 65–93 (2018).
2. Hung, A. M., Mousavi, M., Fini, E. H. Implication of wax on hindering self-healing processes in bitumen. *Applied Surface Science*. **523**, 146449 (2020).
3. Lv, Q. et al. Investigating the asphalt binder/mastic bonding healing behavior using bitumen bonding strength test and X-ray Computed Tomography scan. *Construction and Building Materials*. **257**, 119504 (2020).
4. Liang, B. et al. Review on the self-healing of asphalt materials: Mechanism, affecting factors, assessments and improvements. *Construction and Building Materials*. **266 (part A)**, 120453 (2021).
5. Xu, S. et al. Self-healing asphalt review: From idea to practice. *Advanced Materials Interfaces*. **5**, 1800536 (2018).
6. Tabaković, A., Schlangen, E. in *Self-healing Materials* 10.1007/12_2015_335 *Advances in Polymer Science* Ch. Chapter 335, 285–306 (2015).
7. García, Á. Self-healing of open cracks in asphalt mastic. *Fuel*. **93**, 264–272 (2012).
8. Karimi, M. M., Amani, S., Jahanbakhsh, H., Jahangiri, B., Alavi, A. H. Induced heating-healing of conductive asphalt concrete as a sustainable repairing technique: A review. *Cleaner Engineering and Technology*. **4** (2021).
9. Gulisano, F., Gallego, J. Microwave heating of asphalt paving materials: Principles, current status and next steps. *Construction and Building Materials*. **278**, 121993 (2021).
10. García, Á., Schlangen, E., Ven, M. v. d., Bochove, G. v. Optimization of composition and mixing process of a self-healing porous asphalt. *Construction and Building Materials*. **30**, 59–65 (2012).
11. Aguirre, M. A., Hassan, M. M., Shirzad, S., Daly, W. H., Mohammad, L. N. Micro-encapsulation of asphalt rejuvenators using melamine-formaldehyde. *Construction and Building Materials*. **114**, 29–39 (2016).
12. Su, J.-F., Qiu, J., Schlangen, E., Wang, Y.-Y. Experimental investigation of self-healing behavior of bitumen/microcapsule composites by a modified beam on elastic foundation method. *Materials and Structures*. **48** (12), 4067–4076 (2014).
13. Yoo, D. Y., Kim, S., Kim, M. J., Kim, D., Shin, H. O. Self-healing capability of asphalt concrete with carbon-based materials. *Journal of Materials Research and Technology-Jmr&T*. **8** (1), 827–839 (2019).
14. Qin, Z., Jung, G. S., Kang, M. J., Min Jeong, M. J. The mechanics and design of a lightweight three-dimensional graphene assembly. *Science Advances*. **3** (1), e1601536 (2017).
15. Jung, G. S., Yeo, J., Tian, Z., Qin, Z., Buehler, M. J. Unusually low and density-insensitive thermal conductivity of three-dimensional gyroid graphene. *Nanoscale*. **9** (36), 13477–13484 (2017).
16. Campbell, P. G., Worsley, M. A., Hiszpanski, A. M., Baumann, T. F., Biener, J. Synthesis and functionalization of 3D nano-graphene materials: Graphene aerogels and graphene macro

668 assemblies. *Journal of Visualized Experiments: JoVE*. (105), e53235 (2015).
669 17. Li, H. et al. Induction heating and healing behaviors of asphalt concretes doped with
670 different conductive additives. *Advances in Materials Science and Engineering*. **2019**, 1–10
671 (2019).
672 18. Moreno-Navarro, F., Sol-Sánchez, M., Gámiz, F., Rubio-Gámez, M. C. Mechanical and
673 thermal properties of graphene modified asphalt binders. *Construction and Building Materials*.
674 **180**, 265–274 (2018).
675 19. Liu, J., Hao, P., Dou, Z., Wang, J., Ma, L. Rheological, healing and microstructural properties
676 of unmodified and crumb rubber modified asphalt incorporated with graphene/carbon black
677 composite. *Construction and Building Materials*. **305**, 124512 (2021).
678 20. Wang, R., Qi, Z., Li, R., Yue, J. Investigation of the effect of aging on the thermodynamic
679 parameters and the intrinsic healing capability of graphene oxide modified asphalt binders.
680 *Construction and Building Materials*. **230**, 116984 (2020).
681 21. Gulisano, F., Crucho, J., Gallego, J., Picado-Santos, L. Microwave healing performance of
682 asphalt mixture containing Electric Arc Furnace (EAF) slag and Graphene Nanoplatelets (GNPs).
683 *Applied Sciences*. **10** (4), 1428 (2020).
684 22. Li, C., Wu, S., Chen, Z., Tao, G., Xiao, Y. Improved microwave heating and healing properties
685 of bitumen by using nanometer microwave-absorbers. *Construction and Building Materials*.
686 **189**, 757–767 (2018).
687 23. Varma, R., Balieu, R., Kringos, N. A state-of-the-art review on self-healing in asphalt
688 materials: Mechanical testing and analysis approaches. *Construction and Building Materials*.
689 **310**, 125197 (2021).
690 24. Lau, D., Jian, W., Yu, Z., Hui, D. Nano-engineering of construction materials using
691 molecular dynamics simulations: Prospects and challenges. *Composites Part B: Engineering*.
692 **143**, 282–291 (2018).
693 25. Jian, W., Lau, D. Creep performance of CNT-based nanocomposites: A parametric study.
694 *Carbon*. **153**, 745–756 (2019).
695 26. Wang, X. Q., Jian, W., Buyukozturk, O., Leung, C. K. Y., Lau, D. Degradation of epoxy/glass
696 interface in hygrothermal environment: An atomistic investigation. *Composites Part B:*
697 *Engineering*. **206**, 108534 (2021).
698 27. Jian, W., Lau, D. Understanding the effect of functionalization in CNT-epoxy
699 nanocomposite from molecular level. *Composites Science and Technology*. **191**, 108076 (2020).
700 28. Hao, H., Tam, L.-h., Lu, Y., Lau, D. An atomistic study on the mechanical behavior of
701 bamboo cell wall constituents. *Composites Part B: Engineering*. **151**, 222–231 (2018).
702 29. Qin, R., Zhou, A., Yu, Z., Wang, Q., Lau, D. Role of carbon nanotube in reinforcing
703 cementitious materials: An experimental and coarse-grained molecular dynamics study.
704 *Cement and Concrete Research*. **147**, 106517 (2021).
705 30. Jian, W., Wang, X., Lu, H., Lau, D. Molecular dynamics simulations of thermodynamics and
706 shape memory effect in CNT-epoxy nanocomposites. *Composites Science and Technology*. **211**,
707 108849 (2021).
708 31. Jing, C. et al. Regenerated and rotation-induced cellulose-wrapped oriented CNT fibers
709 for wearable multifunctional sensors. *Nanoscale*. **12** (30), 16305–16314 (2020).

710 32. Yazdandoost, F., Mirzaeifar, R., Qin, Z., Buehler, M. J. Multiscale mechanics of the lateral
711 pressure effect on enhancing the load transfer between polymer coated CNTs. *Nanoscale*. **9**
712 (17), 5565–5576 (2017).
713 33. Doblack, B. N., Allis, T., Davila, L. P. Novel 3D/VR interactive environment for MD
714 simulations, visualization and analysis. *Journal of Visualized Experiments: JoVE*. (94) (2014).
715 34. Xu, M. et al. Improved chemical system for molecular simulations of asphalt. *Energy &*
716 *Fuels*. **33** (4), 3187–3198 (2019).
717 35. Xu, G., Wang, H. Molecular dynamics study of oxidative aging effect on asphalt binder
718 properties. *Fuel*. **188**, 1–10 (2017).
719 36. Nie, F., Jian, W., Lau, D. An atomistic study on the thermomechanical properties of
720 graphene and functionalized graphene sheets modified asphalt. *Carbon*. **182**, 615–627 (2021).
721 37. Cui, B., Gu, X., Hu, D., Dong, Q. A multiphysics evaluation of the rejuvenator effects on
722 aged asphalt using molecular dynamics simulations. *Journal of Cleaner Production*. **259** (2020).
723 38. Sun, W., Wang, H. Self-healing of asphalt binder with cohesive failure: Insights from
724 molecular dynamics simulation. *Construction and Building Materials*. **262**, 120538 (2020).
725 39. He, L. et al. Self-healing behavior of asphalt system based on molecular dynamics
726 simulation. *Construction and Building Materials*. **254**, 119225 (2020).
727 40. Sun, D., Lin, T., Zhu, X., Tian, Y., Liu, F. Indices for self-healing performance assessments
728 based on molecular dynamics simulation of asphalt binders. *Computational Materials Science*.
729 **114**, 86–93 (2016).
730 41. Li, D. D., Greenfield, M. L. Chemical compositions of improved model asphalt systems for
731 molecular simulations. *Fuel*. **115**, 347–356 (2014).
732 42. Redelius, P., Soenen, H. Relation between bitumen chemistry and performance. *Fuel*. **140**,
733 34–43 (2015).
734 43. Schulze, M., Lechner, M. P., Stryker, J. M., Tykwinski, R. R. Aggregation of asphaltene
735 model compounds using a porphyrin tethered to a carboxylic acid. *Organic & Biomolecular*
736 *Chemistry*. **13** (25), 6984–6991 (2015).
737 44. Robertson, A. W., Warner, J. H. Atomic resolution imaging of graphene by transmission
738 electron microscopy. *Nanoscale*. **5** (10), 4079–4093 (2013).
739 45. Yang, L., Zhou, D., Kang, Y. Rheological properties of graphene modified asphalt binders.
740 *Nanomaterials (Basel)*. **10** (11), 2197 (2020).
741 46. Zeng, W. B., Wu, S. P., Pang, L., Sun, Y. H., Chen, Z. W. The utilization of graphene oxide in
742 traditional construction materials: Asphalt. *Materials*. **10** (1), 48 (2017).
743 47. Li, R., Xiao, F., Amirkhanian, S., You, Z., Huang, J. Developments of nano materials and
744 technologies on asphalt materials – A review. *Construction and Building Materials*. **143**, 633–
745 648 (2017).
746 48. Yu, T., Zhang, H., Wang, Y. Multi-gradient analysis of temperature self-healing of asphalt
747 nano-cracks based on molecular simulation. *Construction and Building Materials*. **250**, 118859
748 (2020).
749 49. Gao, C., Liu, T., Shuai, C., Peng, S. Enhancement mechanisms of graphene in nano-58S
750 bioactive glass scaffold: mechanical and biological performance. *Scientific Reports*. **4**, 4712
751 (2014).

50. Maple, J. R., Dinur, U., Hagler, A. T. Derivation of force fields for molecular mechanics and dynamics from ab initio energy surfaces. *Proceedings of the National Academy of Sciences of the United States of America*. **85** (15), 5350–5354 (1988).
51. Xu, M., Yi, J., Feng, D., Huang, Y. Diffusion characteristics of asphalt rejuvenators based on molecular dynamics simulation. *International Journal of Pavement Engineering*. **20** (5), 615–627 (2019).
52. Wang, H., Lin, E., Xu, G. Molecular dynamics simulation of asphalt-aggregate interface adhesion strength with moisture effect. *International Journal of Pavement Engineering*. **18** (5), 414–423 (2017).
53. Yu, J. et al. Insights on the capillary transport mechanism in the sustainable cement hydrate impregnated with graphene oxide and epoxy composite. *Composites Part B: Engineering*. **173** (2019).
54. Zhou, X. et al. Evaluation of thermo-mechanical properties of graphene/carbon-nanotubes modified asphalt with molecular simulation. *Molecular Simulation*. **43** (4), 312–319 (2017).
55. Plimpton, S. Fast parallel algorithms for short-range molecular-dynamics *Journal of Computational Physics*. **117** (1), 1–19 (1995).
56. Stukowski, A. Visualization and analysis of atomistic simulation data with OVITO–the Open Visualization Tool. *Modelling and Simulation in Materials Science and Engineering*. **18** (1), 015012 (2010).
57. Chen, Z., Pei, J., Li, R., Xiao, F. Performance characteristics of asphalt materials based on molecular dynamics simulation–A review. *Construction and Building Materials*. **189**, 695–710 (2018).
58. Sun, D., Sun, G., Zhu, X., Ye, F., Xu, J. Intrinsic temperature sensitive self-healing character of asphalt binders based on molecular dynamics simulations. *Fuel*. **211**, 609–620 (2018).

Figure 1

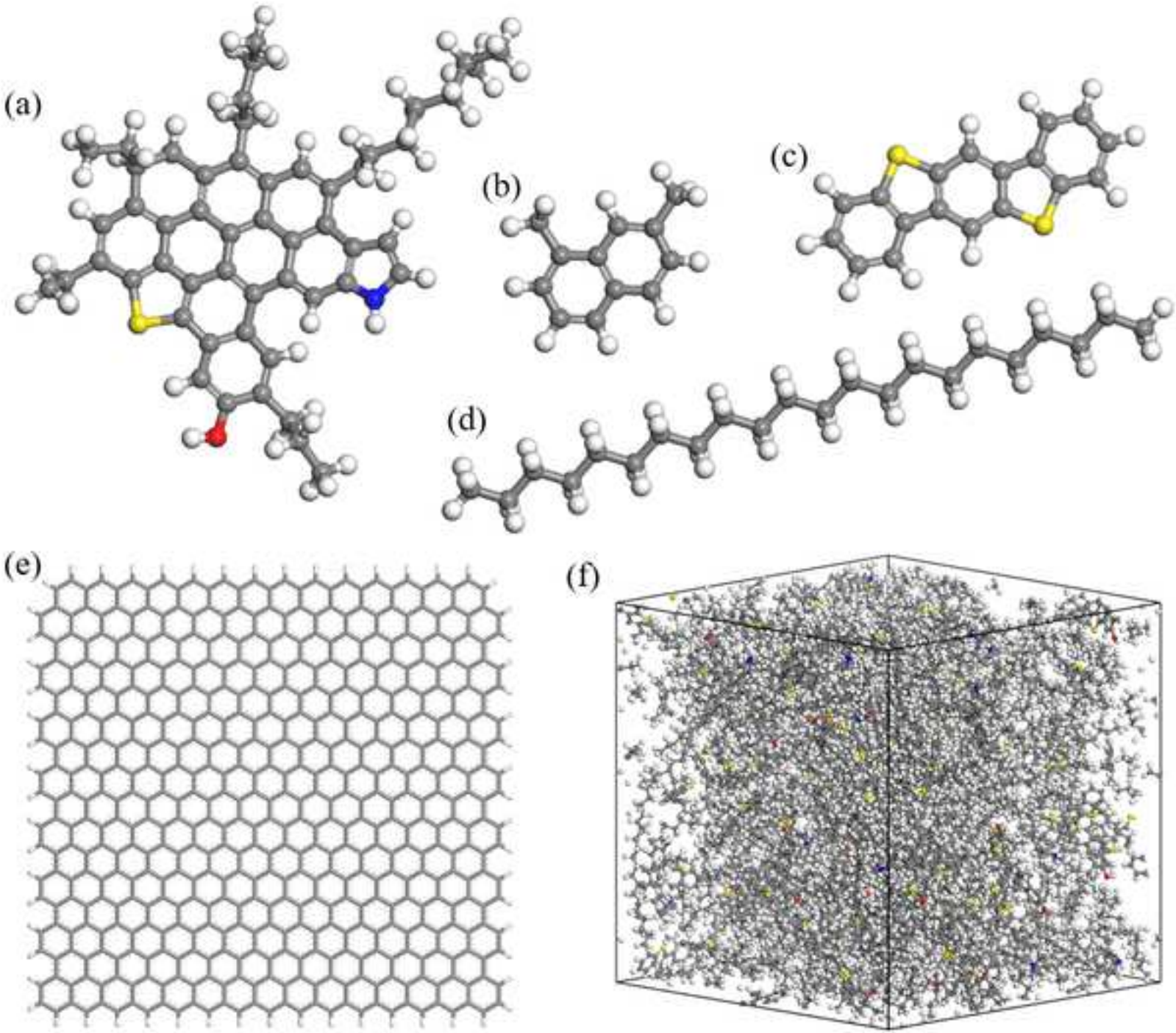

Figure 2

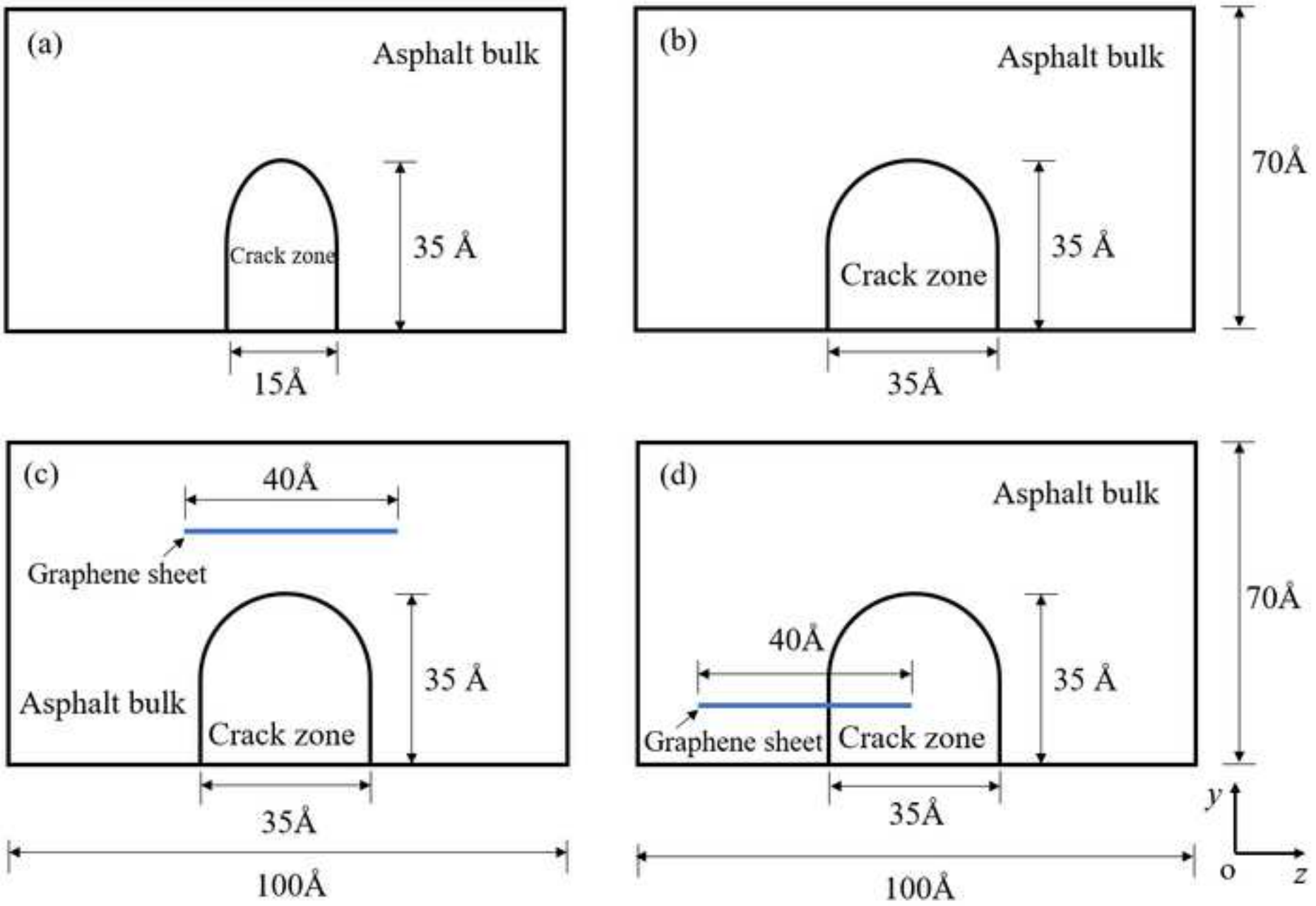

Figure 3 revised

Click here to access/download;Figure;Figure3.tif

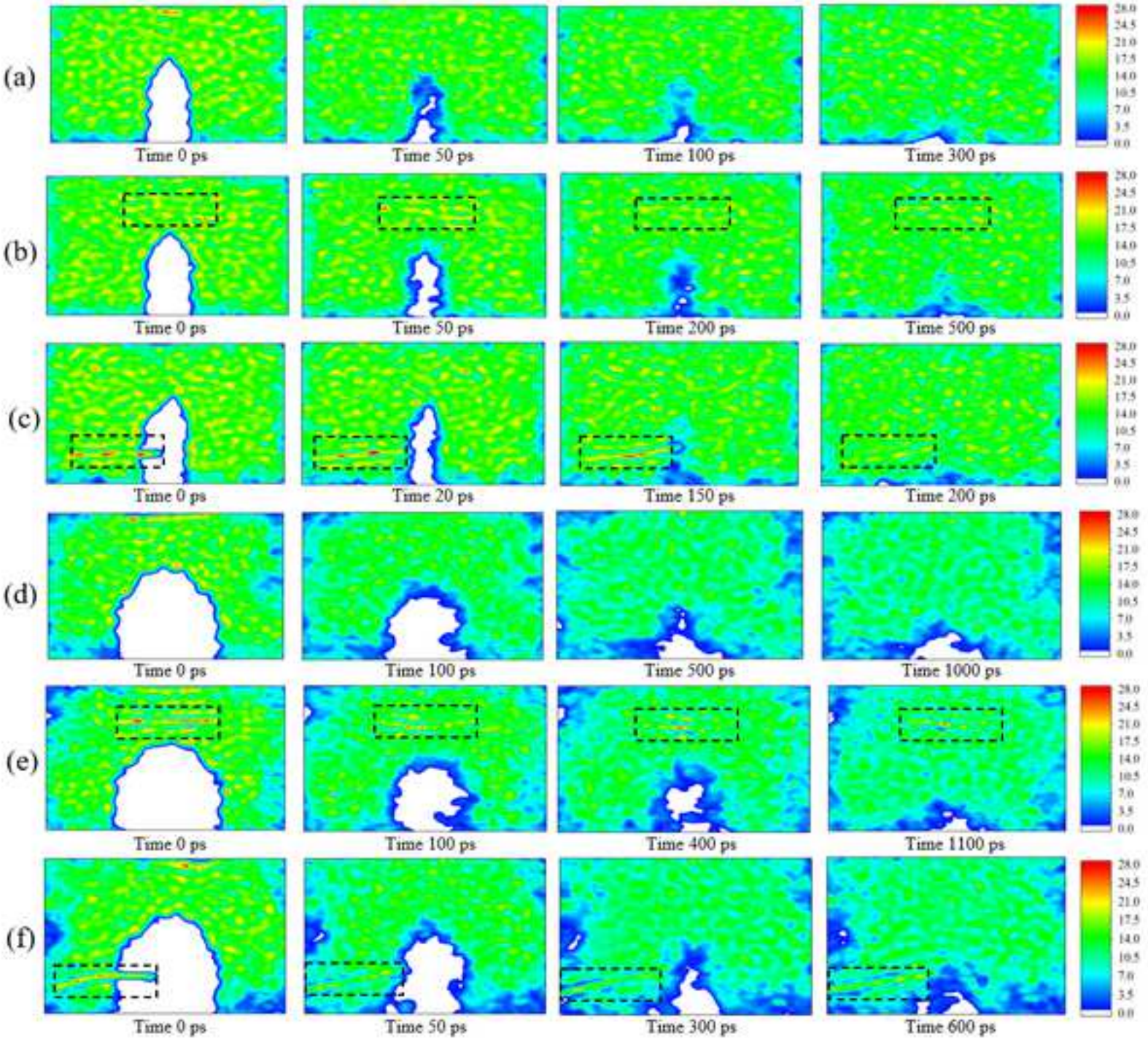

Figure 4

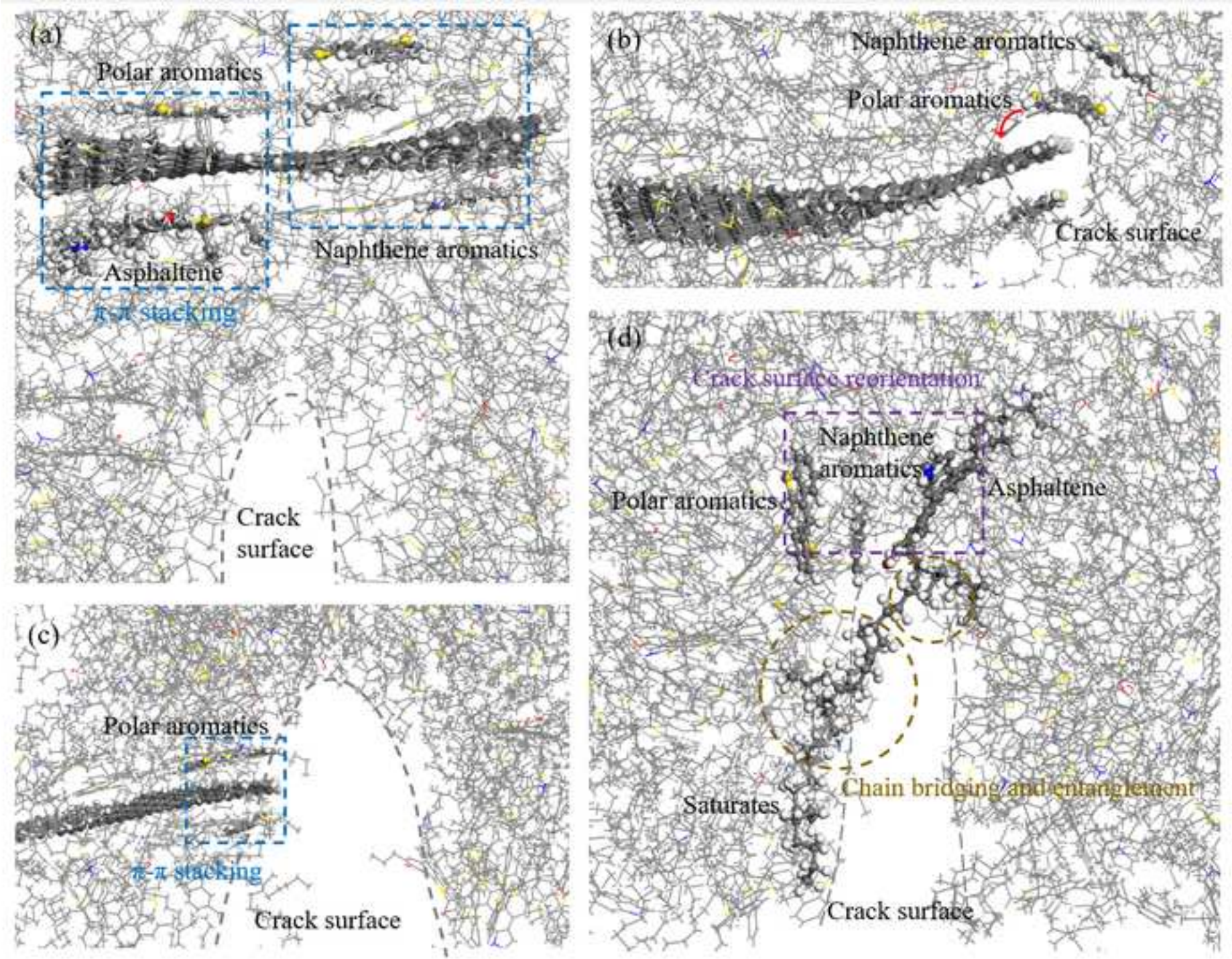

Figure 5

Click here to access/download;Figure;Figure5.tif

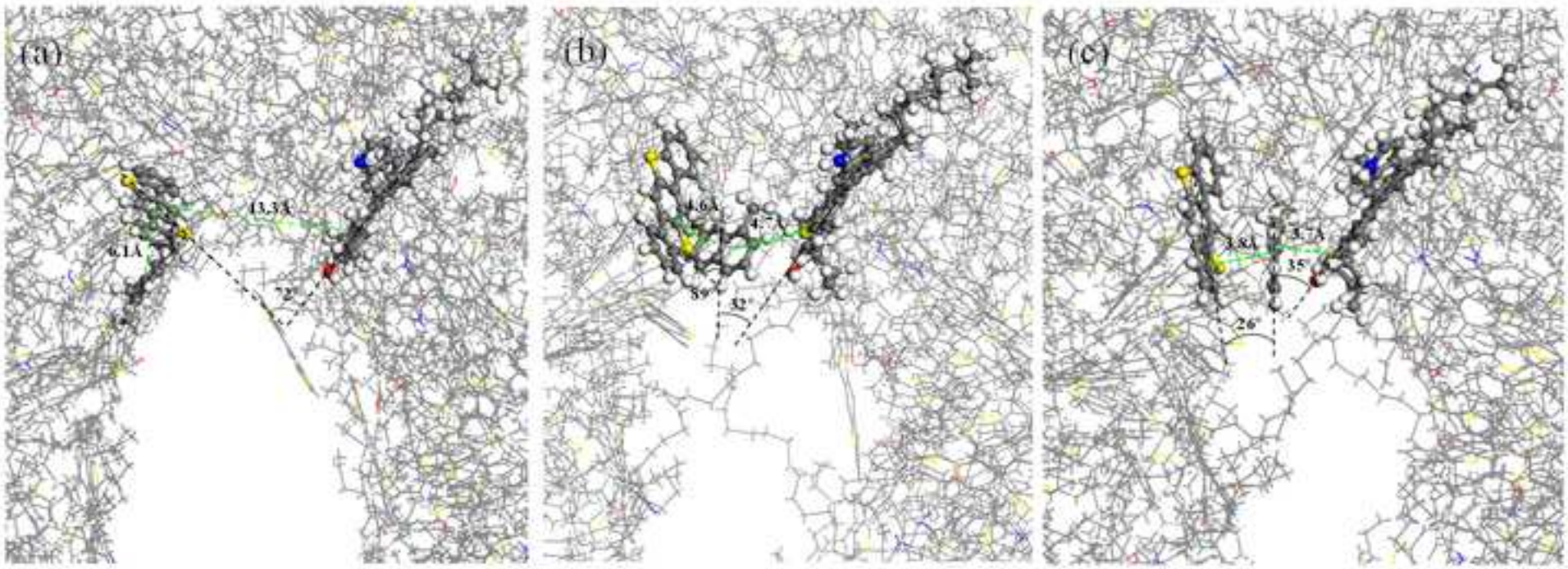

Figure 6 revised

Click here to access/download;Figure;Figure6.tif

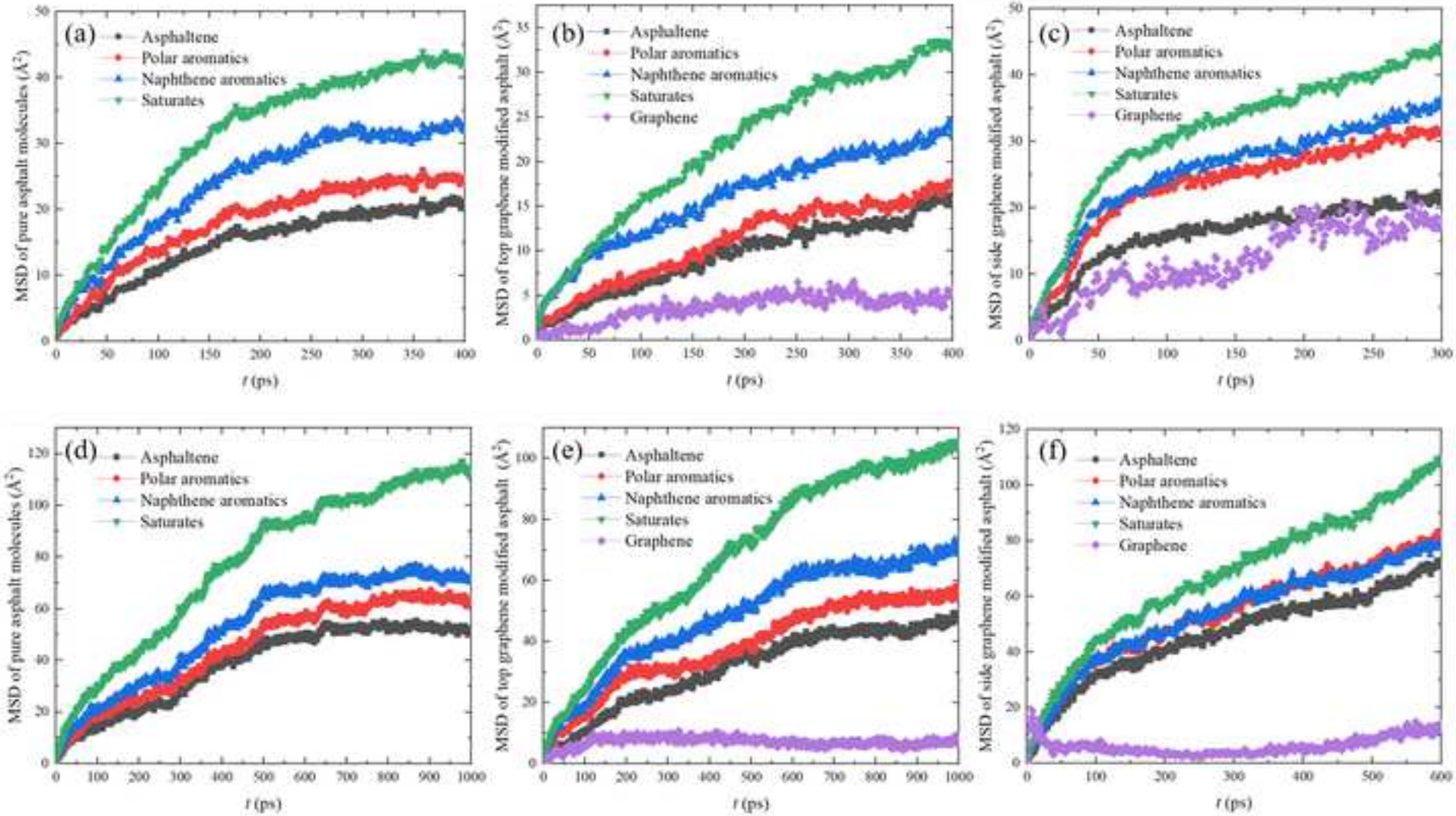

Figure 7

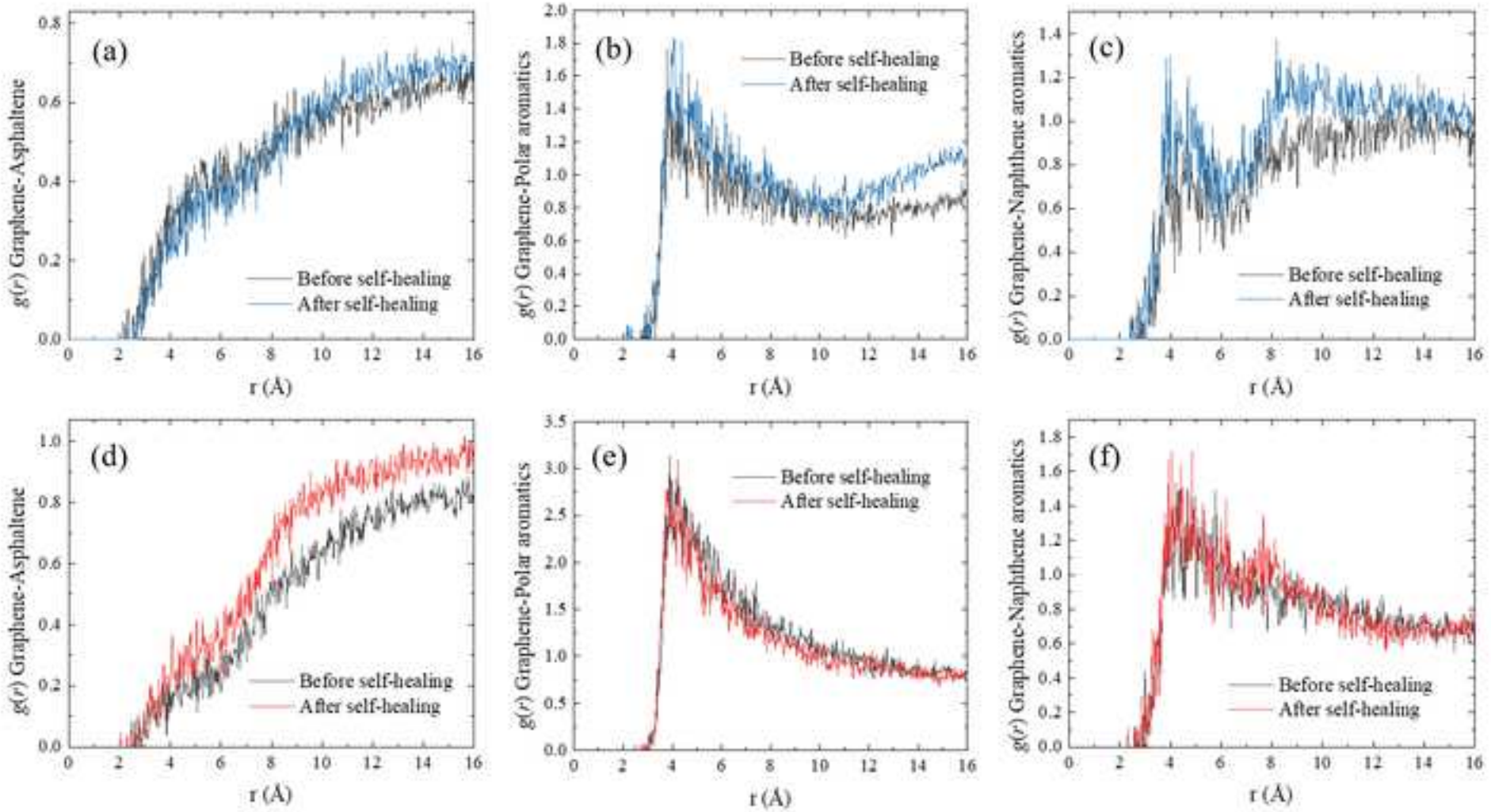

Table 1: Overall components of pure asphalt model and graphene modified asphalt model

Asphalt model	Mass (g/mol)	Chemical formula	Numbers of molecules	Total mass (g/mol)
Asphaltene	754.04	C53H55NOS	43	32423.72
Naphthene aromatic	156.22	C12H12	65	10154.3
Polar aromatic	290.38	C18H10S2	74	21485.16
Saturate	310.59	C22H46	205	63670.95
Asphalt binder			387	127734.13
Graphene	6369.28	C525H63	1	6369.28

Mass fraction (%)
26
8
17
49
100

Responses to Editor

Editor-in-chief

Dear Editor:

We thank you for considering our work for publication in The Journal of Visualized Experiments. According to these comments, we have made revisions to the manuscript accordingly. Detailed responses are included in the attached response file and manuscript. Thank you for your careful review that significantly improves this manuscript.

Sincerely,
Denvid Lau

Editorial comments:

1. The manuscript has been formatted according to the journal style. Please retain the changes (see attached).

Thank you for your effort. All the track-changes are retained in the revised manuscript.

2. Please approve/ respond to specific comments in the manuscript.

Yes, all the specific comments are answered in the revised manuscript.

3. Please describe the various components in the figure in the figure legends in detail.

Yes, the components required in the comment are added to the figure legends in the revised figures and manuscript.

4. Once done, please thoroughly proofread the manuscript.

Yes, the proofreading has been done for the revised manuscript.